Icarus 216 (2011) 10–22

Contents lists available at SciVerse ScienceDirect

Icarus

journal homepage: www.elsevier.com/locate/icarus

The martian mesosphere as revealed by CO_2 cloud observations and General Circulation Modeling

Francisco González-Galindo [a,b,*], Anni Määttänen [c], François Forget [b], Aymeric Spiga [b]

[a] Instituto de Astrofísica de Andalucía, CSIC, Granada, Spain
[b] Laboratoire de Météorologie Dynamique, CNRS/UPMC/IPSL, Paris, France
[c] Laboratoire Atmosphères, Milieux, Observations Spatiales, CNRS/UVSQ/UPMC/IPSL, Verrières-le-buisson, France

ARTICLE INFO

Article history:
Received 25 October 2010
Revised 5 August 2011
Accepted 8 August 2011
Available online 16 August 2011

Keywords:
Mars, Atmosphere
Terrestrial planets
Atmospheres, Structure
Aeronomy

ABSTRACT

Different missions have observed mesospheric clouds on Mars in the last years. The presence of these clouds implies, among other conditions, mesospheric temperatures below CO_2 condensation temperature. We use a General Circulation Model to study the mesospheric temperatures and compare the observed distribution of the mesospheric clouds and the predicted climatology of mesospheric temperatures. Although the model does not usually predict temperatures below condensation for daytime conditions, in some regions the predicted temperatures are close enough to condensation that perturbations caused by small scale processes could produce local excursions below condensation. The location and time of the lowest temperatures predicted by the GCM correspond to a first order with the two observed populations of mesospheric clouds: equatorial clouds observed before and after the Northern summer solstice, and mid-latitude clouds observed around the Northern winter solstice. For the equatorial clouds season, the model predicts temperatures close to condensation at the longitude, latitude, altitude and local time where they have been observed. We find that the diurnal migrating thermal tide and non-migrating tides are at the root of the spatial confinement of the equatorial clouds. For the mid-latitude clouds season, the temperatures predicted by the model at the location of the observed clouds is too high. Stereo observations by two different instruments allow for the determination of the zonal speed of these clouds producing a rare dataset of mesospheric winds. We compare the mesospheric zonal winds predicted by the model with these observations, finding a good agreement, although in some cases the observed variability exceeds that predicted by the model.

1. Introduction

While the formation of CO_2 clouds in the lower martian atmosphere during the polar night is a relatively well-known feature (Pollack et al., 1990; Forget et al., 1998; Pettengill and Ford, 2000; Ivanov and Muhleman, 2001; Colaprete and Toon, 2002; Colaprete et al., 2003; Tobie et al., 2003), it is only recently that the existence of mesospheric CO_2 clouds has been observationally revealed on Mars. In the last few years, several different instruments have observed signatures of these clouds. Their presence was first inferred from TES and MOC observations on board Mars Global Surveyor (Clancy et al., 2004, 2007), and later confirmed by THEMIS-VIS (McConnochie et al., 2005, 2010; Inada et al., 2007) and by different instruments on board Mars Express: SPICAM (Montmessin et al., 2006), PFS (Formisano et al., 2006), OMEGA (Montmessin et al., 2007; Määttänen et al., 2010), and HRSC (Scholten et al., 2010; Määttänen et al., 2010).

These clouds exhibit very exotic dynamics and microphysics: the condensation of the main constituent of the atmosphere is a very rare phenomenon in the Solar System, and in addition to Mars probably happens only on Pluto and Triton. In the case of a near-pure vapor, the latent heat released in condensation is not efficiently carried away from the droplet/crystal in the absence of an inert carrier gas, and thus the latent heat affects the mass fluxes in greater amount than during the condensation of a minor species (as water vapor on the Earth or on Mars). In addition, these clouds might be an incarnation of mesospheric convection (Montmessin et al., 2007; Colaprete et al., 2008; Määttänen et al., 2010) driven by the large latent heat release, even though the real nature of these clouds remains unverified. Furthermore, aerosol dynamical processes of CO_2 happen on Mars in a near-pure vapor and in the so-called kinetic and transition regimes (large Knudsen numbers): these effects need to be taken into account in microphysical descriptions of CO_2 cloud formation.

* Corresponding author at: Instituto de Astrofísica de Andalucía, CSIC, P.O. Box 3004, 18080 Granada, Spain.
E-mail addresses: ggalindo@iaa.es, francisco.gonzalez-galindo@lmd.jussieu.fr (F. González-Galindo).

0019-1035/$ - see front matter © 2011 Elsevier Inc. All rights reserved.
doi:10.1016/j.icarus.2011.08.006

Different ingredients are needed to form a mesospheric CO_2 cloud, among them temperatures low enough to initiate nucleation. In addition, the possible presence of condensation nuclei (CN), greatly facilitating nucleation, is an important factor. The source of possible CN at mesospheric altitudes remains unconfirmed, both on Mars and on the Earth. In any case, it has been shown through nucleation calculations (Määttänen et al., 2010) that heterogeneous nucleation of CO_2 on CN of 1 nm radius requires temperature excursions of 15 K below the condensation temperature at altitudes 80–100 km. Such a CN size is extremely small, so it should give a good estimate of the extreme temperature deviations required in the case of heterogeneous nucleation. Temperature between 5 and 10 K below condensation should be enough to initiate nucleation when realistic CN sizes are considered. Määttänen et al. (2010) concluded also that temperature deviations required for homogeneous nucleation of CO_2 at these altitude would require extreme low temperatures that have never been measured on Mars: thus heterogeneous nucleation remains the most probable pathway of CO_2 cloud formation, unless new observations of vertical profiles (SPICAM/MEx, MCS/MRO, etc.) reveal the existence of extremely cold temperatures at mesospheric altitudes.

These mesospheric clouds provide unprecedented diagnostics of this region of the martian atmosphere. In particular, as stated above, a necessary (but not sufficient) condition for the presence of a CO_2 cloud is that the atmospheric temperature must be lower than the CO_2 condensation temperature. Therefore, the presence of a mesospheric CO_2 cloud implies temperatures below condensation. The spatial and temporal distribution of these clouds can thus be used to map low temperatures in the mesosphere. Mars mesospheric temperatures have been previously measured from Earth (e.g. Clancy and Sandor, 1998), but these measurements lack a good geographical resolution. From orbit, mesospheric temperatures have been measured by SPICAM (Forget et al., 2009) and MCS (Lee et al., 2009). However, SPICAM measurements are not reliable below about 70 km (Forget et al., 2009) and MCS measurements do not go above 80 km. The observation of clouds can therefore provide useful additional information of this altitude region. In addition, in some cases, the use of techniques such as the stereoscopic observations results in determinations of the zonal speed of the clouds, which can be assumed to give an estimate of the speed of the mesospheric winds, not previously measured from orbit. Such information is especially valuable to constrain theoretical models, such as General Circulation Models (GCMs), given the scarcity of data about the martian mesosphere and thermosphere.

Previous studies of these mesospheric clouds have been made using GCMs. Montmessin et al. (2007) showed a correlation between the seasonal behavior of the observed clouds and the daily averaged temperatures predicted at 70 km by the LMD-MGCM, although the predicted temperatures did not allow for CO_2 condensation. The study of Colaprete et al. (2008) focused on calculating the convective potential (so-called CAPE) of the martian atmosphere based on observations and on modeling. Their GCM included CO_2 cloud microphysics, but the model top was at 80 km, which probably had important effects on the predicted temperatures close to the model top and inhibited a correct description of the diurnal thermal tide. This low model top also prevents direct comparisons with SPICAM observations of clouds at about 90–100 km (Montmessin et al., 2006). Colaprete et al. (2008) predicted the presence of clouds around the equator and in the middle latitudes of the Northern hemisphere. However, they failed to reproduce the seasonal and geographical distribution of the clouds already reported by Clancy et al. (2007). The thickest mesospheric clouds are predicted to appear over Tharsis (lon = 100°W) at L_s = 180, a period where mesospheric clouds have not been observed. The example of Colaprete et al. (2008) shows that even with detailed microphysics included, a correct description of the thermal field in the mesosphere is essential to correctly predict the presently fairly well known spatial and temporal distribution of the mesospheric CO_2 clouds.

At present, a larger, 6-martian-year dataset of high-altitude cloud observations is available, including unique measurements of mesospheric winds. A part of this dataset was already used by Määttänen et al. (2010) for a quick-look comparison with the LMD-MGCM. Määttänen et al. (2010) found that the altitude of the areas of minimum temperature predicted by the LMD-MGCM matched the altitude of the clouds, even if the predicted temperatures were not low enough to allow for saturation. Also the wind speed inferred from HRSC observations for the L_s = 0–30 period were found to be in good agreement with the atmospheric wind speeds predicted by the LMD-MGCM.

We do not aim here to simulate the formation of the clouds, as our model does not include the sophisticated microphysics necessary to do so. We will focus on one of the ingredients of the recipe of the CO_2 mesospheric clouds: whether or not the large-scale temperatures and winds predicted by the LMD-MGCM are in agreement with the information provided by the observations of mesospheric clouds. This strong focus will leave necessarily out other ingredients important for the formation of the CO_2 clouds, such as the presence of condensation nuclei and detailed microphysical processes. However, we think this study can be useful both to validate the model and to shed light over the possible relationships between the observed climatology of the clouds and the large-scale atmospheric temperature and circulation. Our goal is to investigate if the particular geographical and seasonal distribution of the observed clouds is related to similar tendencies found in the simulated temperatures, and if so, to study which physical processes produce that distribution. In particular, we want to verify if the diurnal thermal tide has an important role in determining the observed distribution of the clouds, as already suggested by Clancy et al. (2007), and to examine which other physical and/or dynamical processes can have an influence.

This paper is divided into six sections. In Section 2 we summarize the different sets of observations of mesospheric CO_2 clouds. In Section 3 we describe the main tool used in this work, the LMD-MGCM, and the characteristics of the simulations. In Section 4 we compare the temperatures predicted by the model with the constrains imposed by the observations of CO_2 clouds, and use the model to better understand some characteristics of the observed clouds. In Section 5 we compare the winds predicted by the LMD-MGCM with those measured by stereo observations by THEMIS and HRSC. In the final section we present the conclusions of the study.

2. Summary of CO_2 cloud observations

As stated in Section 1, several different instruments have detected CO_2 mesospheric clouds on Mars. We will summarize here the main features of each dataset, and identify the main tendencies that can be extracted from these observations.

The first indications of the possibility of mesospheric clouds in the martian atmosphere came from the Mariner missions (James et al., 1992; Clancy and Sandor, 1998) and, more recently, from the thermal profiles obtained by ground-based submillimeter observations and during the Pathfinder entry profile (Clancy and Sandor, 1998), which show temperature below CO_2 condensation at some altitudes. However, the first systematic detections of these high altitude clouds come from MGS TES (solarband channel) and MOC limb profiles that are described in Clancy et al. (2004, 2007). The observations, obtained during martian years (MY) 24–26, are restricted to a small Local Time (LT) range in the dayside, about LT = 13–15, due to the characteristics of the MGS orbit. Clouds are

found to appear on narrow altitude (70–75 km), latitude (10°S–10°N) and longitude (20°E–20°W and 70–110°W) ranges, and in periods before or after aphelion (L_s = 71°), with maximum occurrence at L_s = 20–35° and a secondary maximum at L_s = 145–160°.

Mesospheric clouds have been observed by different instruments on board Mars Express. Two of them have also allowed their unambiguous identification as CO_2 clouds, on the basis of their spectral features (OMEGA, Montmessin et al., 2007) and the comparison with simultaneous temperature profiles (SPICAM, Montmessin et al., 2006).

OMEGA has detected about 60 mesospheric clouds during MY 27–29. These observations are summarized in Montmessin et al. (2007) for MY 27 and Määttänen et al. (2010) for MY 27–29. As for TES solarband, OMEGA only allows for dayside observations, with most of the detections of clouds at LT ≈ 14–16, although there are some observations also in early morning (LT around 8–9). Clouds are observed by OMEGA mostly at longitudes between 150°W and 10°E and latitudes between 20°S and 20°N. Clouds appear around L_s = 0° and are present until L_s = 60°. No clouds are detected between $L_s \approx 60°$ and 90°. The clouds reappear between L_s = 90–120° and definitively disappear after this time, with one exception very late in autumn at northern mid-latitudes at L_s = 250°. However, the uneven sampling of OMEGA in latitude and L_s has to be kept in mind when studying this seasonal behavior. Although OMEGA nadir observations do not in general allow measurement of the cloud altitude, in two of the cases the detection of the cloud shadow has allowed for an estimation of their altitude of about 80 km.

HRSC has also imaged mesospheric clouds. For MY 27 and 28, HRSC images have only been checked in the orbits where OMEGA observed clouds, showing five detections of the same clouds by the two different instruments (Määttänen et al., 2010). For the beginning of MY 29, a more detailed analysis of HRSC data has been performed, allowing to detect about 20 clouds, some of them (14) not observed by OMEGA (Scholten et al., 2010). As in the previous cases, the observations can only be made during daytime. The distribution of the clouds is similar to the ones obtained by MGS and OMEGA: clouds are longitudinally, latitudinally and seasonally confined. The special stereo imaging capability of HRSC, and in particular the use of different viewing angles for each of the filters, allows to estimate the altitude of the cloud and also its speed in the zonal direction (perpendicular to the satellite ground track). The clouds are mainly found in an altitude range between approximately 60 and 85 km, and they usually move westward, with speeds ranging between 20 and 100 m/s. More details about the instrument and the observations can be found in Scholten et al. (2010).

The third instrument on board Mars Express that has detected mesospheric clouds, inferred to be composed of CO_2 on the basis of simultaneous temperature profile retrieval, is SPICAM. Montmessin et al. (2006) reported the detection of four clouds using the technique of stellar occultation. This technique has mostly been used on the nightside of the planet. The four clouds were found at around L_s = 135°, in the low latitudes of the Southern hemisphere, and around midnight. The altitude of the clouds varied between 90 and 100 km. Moreover, the same technique of stellar occultation allows SPICAM to measure temperature profiles in the mesosphere (Forget et al., 2009). During MY 27, about 45 profiles with subfreezing temperature (up to 24 K below condensation) have been found. Many of these profiles were detected in the northern summer, consistently with the SPICAM cloud observations and with the detections by other instruments. Temperatures below CO_2 condensation are mostly found at around 100 km of altitude. However, Forget et al. (2009) did not find any clear tendency in the longitudinal distribution of the observations of subfreezing temperatures, although a wave number 2 structure with minimum temperature at 90°W and 90°E would be consistent with the observations.

Mars Odyssey started its mission in 2001 and the visible channels of the THEMIS instrument on board (THEMIS-VIS) have reportedly observed high-altitude clouds (McConnochie et al., 2005, 2010; Inada et al., 2007). THEMIS-VIS images can be used in a similar manner to HRSC (same location imaged through different filters at slightly different times) to extract information on the cloud altitude and speed. THEMIS-VIS observed equatorial clouds between L_s = 26° and 120° and showed evidences of the existence of the mid-latitude clouds (McConnochie et al., 2005, 2010) also seen by OMEGA and HRSC (Määttänen et al., 2010). THEMIS-VIS observations are limited to local time 16–18. THEMIS-VIS observed mid-latitude clouds in twilight (Sun below local horizon but still illuminating the high-altitude clouds) only in the Northern hemisphere, whereas OMEGA and HRSC observed one cloud in the southern mid-latitudes as well. The northern mid-latitude clouds were observed by THEMIS-VIS at L_s = 200–300° and by OMEGA at L_s = 246.3°. McConnochie et al. (2010) modeled the cloud radiances for the equatorial clouds with a radiative transfer model: based on the results of opacity and condensed mass they concluded that the equatorial clouds were composed of CO_2 ice crystals. The effective radii were 0.1 and 1.5 μm and opacities 0.2 and 0.5, in agreement with the values obtained by the shadow observations of OMEGA (Montmessin et al., 2007; Määttänen et al., 2010), with the exception of the small particles of 0.1 μm, which fit better with the SPICAM observations of the nighttime clouds at higher altitudes (Montmessin et al., 2006). However, THEMIS-VIS observations do not provide any information about the composition of mid-latitude clouds.

To summarize, four different instruments have observed CO_2 mesospheric clouds during the daytime and one other instrument has observed these clouds (and also mesospheric temperatures below CO_2 condensation) during nighttime. Two populations of daytime clouds are found: equatorial clouds, located in a small latitudinal range around the equator (20°S–20°N), between about L_s = 0–180° (with one occurrence at L_s = 330°), and mid-latitude clouds, mostly between L_s = 200–300° in the Northern hemisphere and one occurrence at L_s = 54° in the Southern hemisphere. All these daytime clouds appear only in restricted longitudinal ranges. The observations of nighttime clouds and profiles with subcondensation temperature are concentrated between L_s = 90–150° and L_s = 320–360°, with only two exceptions, and mostly in the mid-latitudes of the winter hemisphere. However, it has to be kept in mind, especially for the nighttime observations, that the spatial and seasonal coverage of the different instruments is far from complete. The typical altitude of daytime clouds is about 70 km, while for the nighttime clouds this altitude is of about 100 km. These features are summarized in Table 1, and the latitude-L_s and latitude–longitude distribution of the clouds can be seen in Fig. 1a and b, respectively.

In what follows, we will study the mesospheric temperatures predicted by the LMD-MGCM and its variability, and try to establish a link between the observed climatology of the clouds and the simulated climatology of mesospheric temperatures. If such a connection is found, we will try to understand which physical processes are behind the structure of the simulated temperatures (and thus likely of the distribution of the observed clouds). In particular we want to address the different questions opened by the observations: Why these clouds are higher during the night (about 100 km) than during the day (80 km)? Why are they confined to a small latitudinal range? Why do the daytime clouds appear preferentially at a restricted longitudinal range? Why do the clouds present such a strong seasonal dependence? Again, we want to remind that we do not try to model the formation of CO_2 clouds, but only the large-scale atmospheric state and circulation that can provide the necessary conditions to enable CO_2 cloud formation.

Table 1
Preferential local time, altitude, latitude, longitude and season location of the CO_2 clouds (and profiles with temperature below condensation, in the case of SPICAM), observed by different instruments.

Instrument	Local time	Altitude (km)	Latitude range	Longitude range	L_s
MGS TES	13–15	70–75	10S–10N	20E–20W; 70W–110W	0–50°; 110–170°
OMEGA	14–16	80	Mostly 20S–20N	10E–20W; 50W–120W	0–60°; 90–140°
HRSC	15–16	60–80	10S–10N	20E–20W; 70W–100W	5–60°; 95–115°
SPICAM	0–1	100	Var	Var	90–150°; 300–360°
THEMIS-VIS	16–18	45–80	20S–50N	260–340E	20–50°; 110–120°; 200–300°

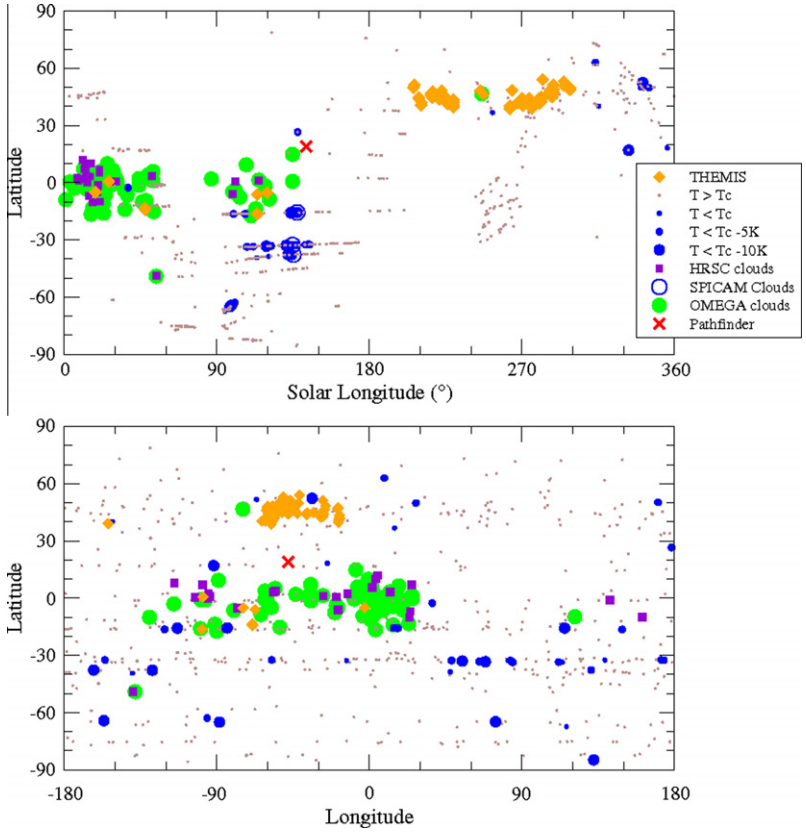

Fig. 1. Top panel: Latitude–season distribution of the mesospheric clouds observed by SPICAM (empty circles), OMEGA (grey stripes), HRSC (magenta squares) and THEMIS-VIS (orange diamonds), and of profiles showing subcondensation observed by Pathfinder (red cross) and SPICAM (blue points). The locations of SPICAM profiles with temperatures always above condensation are shown by grey points. Lower panel: Like top panel, but for the latitude–longitude distribution.

3. Description of the model and the simulations

The LMD-MGCM has already been described elsewhere (Forget et al., 1999; Angelats i Coll et al., 2005; González-Galindo et al., 2009). Briefly, it is a model that solves the primitive equations of hydrodynamics on a sphere by a grid point discretization. It includes the radiative effects of CO_2 and dust, as well as a CO_2 condensation scheme, a water cycle and different parameterizations for sub-grid scale processes (Forget et al., 1999). By adding parameterizations for the physical processes important in the upper atmosphere, the LMD-MGCM has been extended to the thermosphere, becoming a ground-to-exosphere GCM. In particular, the NIR radiative transfer including corrections due to NLTE effects, the heating due to the absorption of UV solar radiation, the thermal conduction, the molecular diffusion and the photochemistry of the rarefied upper atmosphere are now included in the model (González-Galindo et al., 2009).

For this work, we use a simulation of a full martian year. Our goal is to find the location of the areas of minimum mesospheric temperatures predicted by the model, and study its seasonal evolution. We will also focus on the seasons at which most of the CO_2 clouds have been observed, to study the variations with local time, longitude and latitude of those areas of minimum temperature in the mesosphere. For this purpose, we have divided the martian year in 12 intervals of 30 degrees of L_s ("months"). In each of them the results are averaged keeping the diurnal variability. More details about this procedure can be found in González-Galindo et al. (2009).

A dust climatology as observed by TES during MY 24 is prescribed to allow for a realistic simulation of the temperatures. This is considered to be a typical martian year without a global dust storm, and should be appropriate to simulate the conditions during MY 24, MY 26, MY 27 and MY 29, and the periods outside dust storm season (before about $L_s = 180°$) for MY 25 and MY 28. Of course, this dust scenario is not valid for the study of the dust storm periods of MY 25 and MY 28, given that the occurrence of global dust storms strongly modifies the thermal structure of the martian atmosphere. Most of the observations of the clouds have been made in periods where our dust scenario should be valid.

A UV heating efficiency of 16% and a CO_2–O quenching rate of 3×10^{-12} cm^3/s, as well as a solar flux appropriate for solar average

conditions, are used. A more detailed discussion about the choice of these input conditions can be found in Section 3 of González-Galindo et al. (2009).

An important difference with respect to the model described in Forget et al. (1999) and González-Galindo et al. (2009) is that for this simulation we have deactivated the release of latent heat when the temperature falls below CO_2 condensation in the upper atmosphere (for pressures lower than 0.1 Pa). This allows the development of cold pockets in the mesosphere of Mars where temperature can fall below CO_2 condensation.

4. Temperatures: observational constrains and GCM results

4.1. Mesospheric temperatures in the LMD-MGCM: seasonal and latitudinal variability

Previous studies (Montmessin et al., 2007) have tried to compare the seasonal occurrence of CO_2 clouds with the seasonal variability of mesospheric temperatures predicted by the LMD-MGCM, finding a good correlation between them, although the daily averaged temperatures did not allow for CO_2 condensation. Recently, Määttänen et al. (2010) showed the importance of the day-to-day and day–night temperature variations in order to reach temperatures close to (but still higher than) the condensation temperature of CO_2. In this section, we study the seasonal and latitudinal variability of the minimum mesospheric temperatures predicted by the model, and compare it with the seasonal and geographical distribution of the observations of CO_2 clouds.

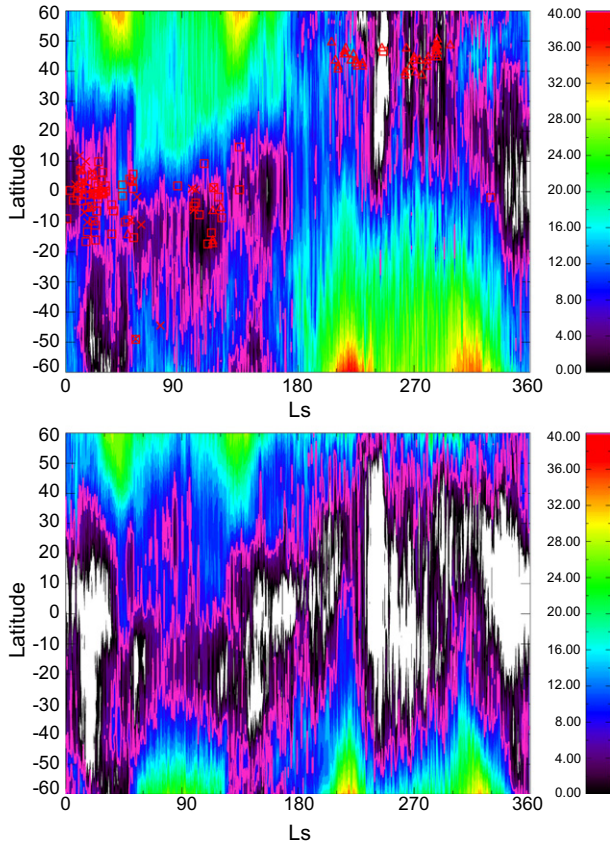

Fig. 2. Minimum T_{diff} predicted by the model as a function of latitude and season: daytime (LT between 6 am and 6 pm, upper panel) and nighttime (LT between 9 pm and 5 am, lower panel). T_{diff} is the difference between the atmospheric temperature and the CO_2 condensation temperature. The white areas indicate regions where the model predicts temperature below CO_2 condensation, while the pink lines indicate areas where predicted temperatures are 7.5 K above condensation. Red symbols show the location of the clouds observed by OMEGA (squares), HRSC (crosses) and THEMIS-VIS (triangles).

In Fig. 2 we represent, for each day of the martian year and for each latitude between 60S and 60N, the minimum value (for all longitudes, altitudes, and local times during daytime (upper panel, local time between 6 am and 6 pm) and nighttime (lower panel, local time between 8 pm and 6 am) of the magnitude $T_{diff} = T - T_{cond}$, where T is the atmospheric temperature and T_{cond} the condensation temperature of CO_2 as given by Washburn (1948): $T_{cond} = -3148/(\ln(0.01T\rho R) - 23.102)$, where ρ is the density in kg/m^3. The areas in white color indicate $T_{diff} < 0$, that is, atmospheric temperatures below CO_2 condensation temperature, while the pink lines indicate those areas where $T_{diff} < 7.5$ K, that is, atmospheric temperature less than 7.5 K above condensation temperature of CO_2. Red symbols indicate OMEGA (squares), HRSC (crosses) and THEMIS-VIS (triangles) observations of daytime clouds.

First, we can clearly see that the model often predicts temperatures below condensation during the night. During the day, it is much more difficult to reach condensation. However, there are substantial areas at dayside where the offset between the atmospheric temperature and the condensation temperature of CO_2 is less than 7.5 K. We will assume here that in these areas the formation of CO_2 clouds is feasible and most probable, because temperature perturbations caused by small scale processes, such as gravity waves, can produce excursions of some individual profiles to temperatures between 5 and 10 K below condensation, enough to allow cloud formation. We will explore further this assumption in Section 4.2.

During the night the model predicts temperature below condensation almost anywhere and anytime. SPICAM observations of clouds and profiles with temperature below condensation concentrate around $L_s = 135°$ in the mid-latitudes of the Southern hemisphere and around $L_s = 330°$ in the mid-latitudes of the Northern hemisphere. This may indicate that the model underestimates the mesospheric temperatures during the night, but it can also be due to the incomplete coverage (both in local time, season, and latitude) of the SPICAM observations.

Focusing on the dayside, it is easy to see that these cold areas concentrate between $L_s = 330$ and 120° close to the equator (divided in two periods, between $L_s = 330$–20° and $L_s = 50$–120°, with warmer temperatures in between), and between $L_s = 210$–300° in the mid-latitudes of the Northern hemisphere. This is similar to the distribution of the two populations of observed clouds described in Section 2. The model also predicts low temperatures south of 40°S, between $L_s = 20°$ and 40°, close to the location of one cloud observed by OMEGA and HRSC. We can say that the distribution of the areas of cold temperatures in the dayside predicted by the LMD-MGCM is, to a first order, in agreement with the observations of CO_2 clouds during daytime.

However, when looking in more detail, some differences between the predictions of the model and the clouds observations arise. Most of the clouds have been observed during the afternoon (local times between 15 and 18), with some observations also during the morning (local times between 7 and 10). The upper panels of Fig. 3 are similar to the upper panel of Fig. 2, but focusing of the LTs where clouds have been observed: between 7 and 10 (left panel) and between 15 and 18 (right panel). In the lower panels, the altitudes of the areas of minimum temperature are shown.

The model predicts lower mesospheric temperatures (and thus higher probabilities of formation of mesospheric clouds) during the morning than during the afternoon. However, most of the clouds have been observed during the afternoon, and only few clouds have been detected during the morning. It should also be kept in mind that most of the instruments that have detected mesospheric clouds are limited to observe in the afternoon due to their orbit geometry.

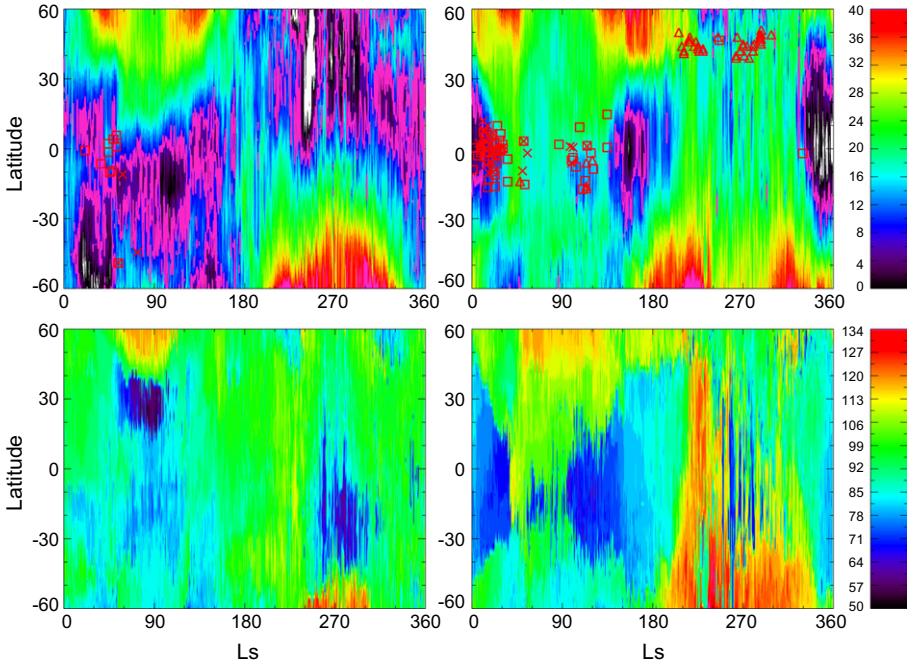

Fig. 3. Upper panels: Same as Fig. 2, but for LT between 7 and 10 (left panel) and between 15 and 18 (right panel). Lower panels: altitude of the minimum T_{diff} predicted by the model as a function of latitude and season for LT between 6 and 9 (left panel) and between 15 and 18 (right panel).

During the morning, mesospheric clouds have been observed between $L_s = 20°$ and 60°, most of them around the equator. At this period, the model predicts temperatures close to condensation around the equator during the morning. The model predicts also low temperatures at this season in the mid-latitudes of the Southern hemisphere, close to the location of two observed clouds. At the locations where clouds have been observed during the morning, minimum temperatures are predicted at altitudes between about 70 and 90 km, while the only three morning clouds for which the altitude has been measured present altitudes between 53 and 87 km.

During the afternoon, the minimum temperatures are predicted by the model close to the equator at different periods: between $L_s = 330–20°$ and between $L_s = 150–180°$, with secondary minima around $L_s = 90–120°$ and $L_s = 240–270°$. The first period of minimum temperatures in the equator seems to end too early in the model (around $L_s = 20°$, while most of the observations of the clouds concentrate between $L_s = 20°$ and 35°). Equatorial clouds have also been observed in the period $L_s = 90–120°$, a period when the model predicts cold temperatures, although colder temperatures are predicted for the period $L_s = 150–180°$, where clouds have not been observed. At these periods where clouds have been observed in the equator, minimum temperatures are predicted by the model at altitudes between around 55 and 80 km, while clouds have been observed at altitudes between 53 and 83 km.

At mid-latitudes of the Northern hemisphere, between $L_s = 210°$ and 300°, the model predicts very cold temperatures (even below CO_2 condensation) during the morning, while clouds have been observed there during the afternoon. Clearly, there is an issue here with the diurnal variability of the temperatures predicted by the model at mid-latitudes during this season. This will be further discussed in Section 4.4.

4.2. Subcondensation temperatures

As can be seen in Fig. 2, the LMD-MGCM only predicts temperature below condensation during daytime in a very small seasonal–latitudinal range around $L_s = 240°$ and lat = 40N, and between $L_s = 330°$ and 360° around the equator, while CO_2 clouds have been observed at different locations and times of the year. Previous work (Forget et al., 2009; González-Galindo et al., 2009) has shown that the LMD-MGCM tends to overestimate the temperatures at the mesopause altitudes, pointing to an underestimation of the 15 μm cooling as a possible reason. The fact that the LMD-MGCM hardly predicts supersaturation during the day might be another indication of this overestimation of temperatures. Tests using a modified 15 μm cooling do not improve the situation, as the simulated temperature decreases only above 100 km, not at the altitudes where CO_2 clouds have been observed during the day. However, we cannot rule out the possibility that the model is overestimating temperatures in the martian mesosphere. One possibility is that the model overestimates the NIR heating rate, essential for the mesospheric thermal balance and that is subject to NLTE effects. An improved parameterization of this process is being developed (López-Valverde et al., 2011), and its future inclusion in the GCM will allow to check its impact on the mesospheric temperatures.

We explore here another possibility. While the GCM has a horizontal grid size of about 200 km, the observed mesospheric clouds have typical sizes about one order of magnitude smaller. The GCM temperatures actually describe an average temperature inside a GCM grid point (typically 200 × 200 km). In reality, small scale processes not resolved by the GCM may modify locally (inside the GCM grid point) the large-scale temperature profiles predicted by the model, producing local excursions below condensation when the large-scale temperatures are close enough to the condensation temperature of CO_2. On the Earth, it has been shown that GCMs predict correctly the areas of low temperature associated with some types of polar stratospheric clouds, but perturbations by gravity waves are necessary to achieve subcondensation temperatures (Noel et al., 2009). Clancy and Sandor (1998) also suggested that gravity waves, in addition to tides, could play a role in producing temperatures low enough to allow the formation of CO_2 clouds.

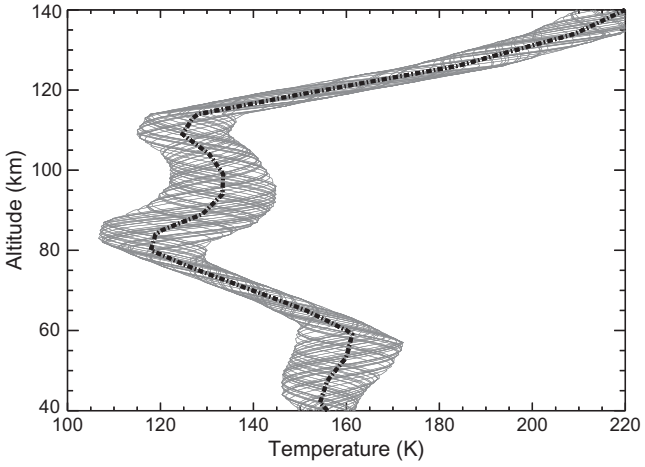

Fig. 4. Temperature profile produced by the LMD-MGCM at $L_s = 0–30°$, lat = 0°, lon = −60° and LT = 16 (thick dashed-dotted line) and perturbations produced by the propagation of gravity waves (thin grey solid lines).

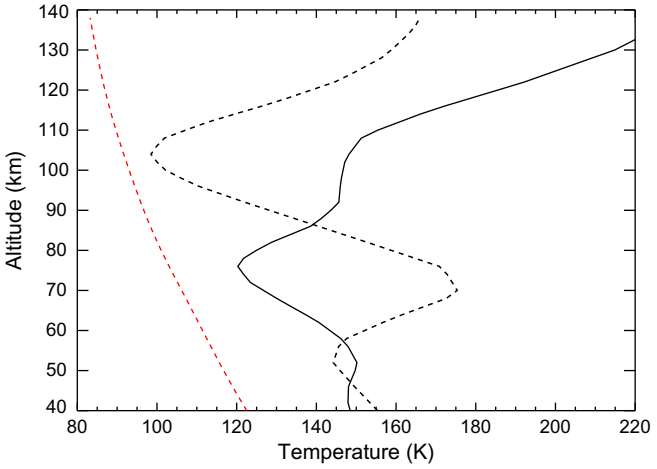

Fig. 5. Temperature profiles obtained from the LMD-MGCM for daytime (LT = 16, solid line) and nighttime (LT = 1, dashed line), and condensation temperature of CO_2 (red dashed line). Each profile corresponds to the average of the period $L_s = 0–30°$, at lon = 0°, lat = 0°.

We want to remind here that the LMD-MGCM includes a parameterization that takes into account the effects of non-resolved gravity waves over the general circulation (Forget et al., 1999), namely the deposition of momentum by gravity wave drag, but the effects of gravity waves over individual temperature profiles are not included. This would need high resolution modeling (i.e. mesoscale models), which is out of the scope of this paper.

To estimate the amplitude of the temperature perturbations produced by gravity waves, we use a simplified model for the excitation and propagation of gravity waves included in the Mars Climate Database and described in Lewis et al. (1999) to produce perturbations to a temperature profile produced by the LMD-MGCM at $L_s = 0°$, lat = 0°, lon = −60° and LT = 16. The results can be seen in Fig. 4, where the dashed-dotted black line represents the GCM profile and the solid grey lines the perturbed profiles produced by the model of gravity wave propagation, for different seed values. We can see that, at about 80 km, the perturbations produced by the propagation of gravity waves are between about 5 and 15 K. This means that for a GCM profile close enough to the condensation temperature of CO_2 (as those in the areas marked with pink lines in Fig. 2, which are less than 7.5 K above condensation), perturbations produced by gravity waves can induce high altitude cooling and hence local temperatures (inside the GCM grid point) can fall some degrees below condensation (up to 7.5 K, considering the case of a 15 K perturbation to a profile 7.5 K above condensation), allowing for the formation of CO_2 clouds. We remind that, following Määttänen et al. (2010), temperatures 15 K below condensation are enough to produce nucleation on 1 nm particles, which can be considered a rather extreme case, and 5–10 K below condensation should be low enough to produce clouds if more realistic nuclei sizes are considered.

The simplified nature of this study must be kept in mind. More detailed studies are needed, ideally using a mesoscale model (Spiga and Forget, 2009) to study the propagation of gravity waves into the martian mesosphere and their effects over the temperatures. Such a study has recently been undertaken (Spiga et al., 2011). Still this simplified study reveals the possibility of a local production of subcondensation temperatures locally, even when the large-scale temperatures are above condensation.

4.3. Equatorial clouds

The observations of the equatorial mesospheric clouds show that they appear only at restricted latitudinal and longitudinal ranges, and that there is a clear difference in their altitude at daytime (about 70–80 km) and at nighttime (about 100 km). We will try here to relate this behavior to the thermal structure of the martian mesosphere as predicted by the LMD-MGCM.

4.3.1. Day–night altitude variation

Fig. 5 shows two typical time-averaged temperature profiles obtained by the LMD-MGCM for the $L_s = 0–30°$ season, at the equator and prime meridian, together with the condensation temperature of CO_2. One of the profiles corresponds to daytime conditions (LT = 16) and the other to nighttime conditions (LT = 1). We can clearly see that the altitude of the minimum temperature is different in both profiles: while for the daytime profile the minimum temperature is found at about 75 km, the nighttime profile presents a minimum of temperature at about 105 km. This coincides well with the altitude of the observed daytime and nighttime clouds.

A similar tendency is shown in Fig. 6, where the difference between the average atmospheric temperature predicted by the LMD-MGCM and the condensation temperature of CO_2 ($T_{\mathrm{diff}} = T_{GCM} - T_{\mathrm{cond}}$) is shown as a function of altitude and local time for the $L_s = 120–150°$ season. Note that at this particular season both daytime and nighttime clouds have been observed. We can see that the altitude of the areas of minimum difference with the condensation temperature of CO_2 changes with local time. Minimum values of T_{diff} are obtained at about 90 km at the end of the night and 60 km at the end of the afternoon. At a given local time, an alternance of areas of maximum and minimum difference of temperature when varying the altitude is obtained, with a vertical wavelength of about 30 km. Note that the minimum T_{diff} (and thus, the maximum probability of having CO_2 clouds) is predicted by the model at the end of the night at about 90 km.

The altitude variation of the minimum of temperature that can be seen in Figs. 5 and 6 is a typical signature of the vertical propagation of the diurnal tide. This mesospheric diurnal tide has been observed in temperature profiles obtained by MCS (Lee et al., 2009) and SPICAM (Forget et al., 2009) and has also been simulated by the LMD-MGCM (Angelats i Coll et al., 2004; González-Galindo et al., 2009) and Mars WRF (Lee et al., 2009). The diurnal thermal tide was proposed as a key mechanism in the formation of these mesospheric clouds by Clancy et al. (2007). The simulated vertical wavelength (about 30 km) is in good agreement with the observations of the diurnal tide (Lee et al., 2009), and also the simulated amplitude (of about 40 K) is in reasonable agreement with the observations (observed semiamplitudes are between 15 and 20 K).

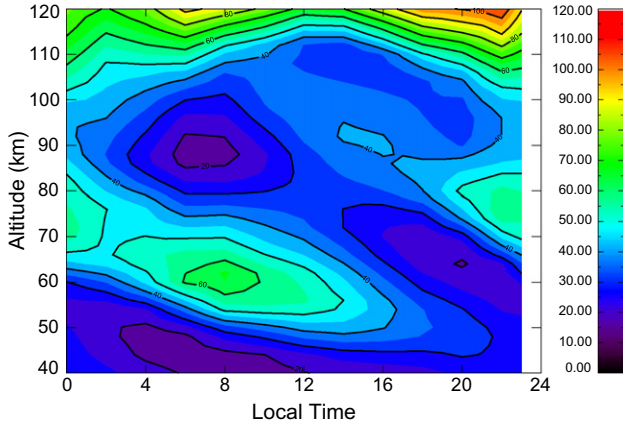

Fig. 6. Difference between the atmospheric temperature and the condensation temperature of CO_2, as a function of altitude and local time. Average over L_s = 120–150°, lon = 0°, lat = 0°.

We can conclude that the day–night variation of altitude of the clouds is very likely linked to the day–night variation of the altitude of the minimum of temperature due to the vertical propagation of the diurnal tide.

4.3.2. Latitudinal and longitudinal distribution

As mentioned in Section 2, the daytime clouds seem to be restricted to narrow latitudinal and longitudinal ranges. Which processes are at the origin of this behavior?

Fig. 7 shows the variation of T_{diff}, defined above, as a function of latitude and altitude, for the L_s = 0–30° season and constant LT = 16. We can clearly see that the minimum temperature for this case is located around the equator, in a latitude range approximately from 20°S to 20°N. This is in agreement with the latitudinal distribution of the CO_2 clouds observed by OMEGA, HRSC and TES at this season and during daytime.

Clancy et al. (2007) already pointed to thermal tides as a key process in the formation of these mesospheric clouds. We represent in Fig. 8 the daily mean temperature for the L_s = 0–30° season (upper panel) and the difference of temperature between midday and midnight (lower panel). At the altitudes where the clouds have been observed and where the model predicts minimum temperatures (between about 60 and 80 km), the daily mean temperature for this season is only marginally lower (less than 5 K) around the equator (lat < 20°, where clouds have been observed) than at latitudes

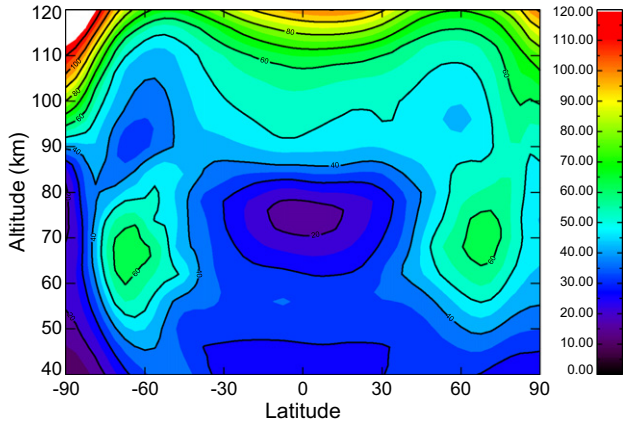

Fig. 7. Latitude–altitude variation of the difference between the predicted temperature and the CO_2 condensation temperature. Average over L_s = 0–30°, LT = 16.

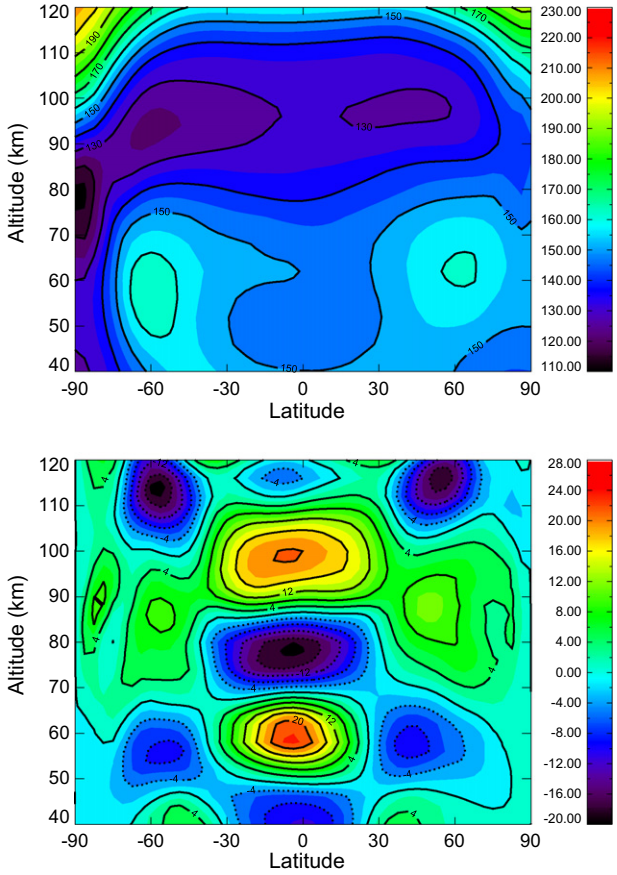

Fig. 8. Latitude–altitude variation of the daily and zonal mean temperature (upper panel) and the midday–midnight temperature difference. L_s = 0–30°, LT = 16.

around 30–40° in both hemispheres (where clouds have not been observed). On the other hand, the day–night temperature difference, which is an indication of the intensity of the diurnal thermal tide, shows a clear maximum around the equator. The amplitude of the diurnal tide decreases strongly with latitude, so that it almost vanishes at latitudes around 30° (where clouds have not been observed). The position of nodes and antinodes in the predicted day–night temperature difference is in good agreement with MCS observations of the diurnal tide at this same season (Lee et al., 2009). We can conclude that the confinement of the areas of low temperature (and likely of the mesospheric clouds) to low latitudes is mostly due to the structure of the diurnal tide, which produces strong departures from the daily mean temperature, with maximum amplitudes around the equator.

Not only do CO_2 clouds appear in a narrow latitudinal range, but their longitudinal range is limited as well. Fig. 9 shows the variation with longitude and altitude of T_{diff} at the equator for the L_s = 0–30° season and constant local time LT = 16. It can be seen that the minimum values of T_{diff} are found between 70 and 80 km in two longitudinal ranges between about 150°W and 40°W and between about 20°W and 20°E. This is in good agreement with the longitudinal location of the clouds observed by HRSC, OMEGA, TES and THEMIS-VIS.

Since heating terms acting at these altitudes (in particular, the heating due to the absorption of NIR radiation by CO_2) are not expected to present a strong variation with longitude at a constant LT, the origin of these longitudinal inhomogeneities has to be elsewhere. Different observations have revealed longitudinal variations of different magnitudes in the upper atmosphere of Mars. The aerobraking of MGS allowed measurement of the atmospheric

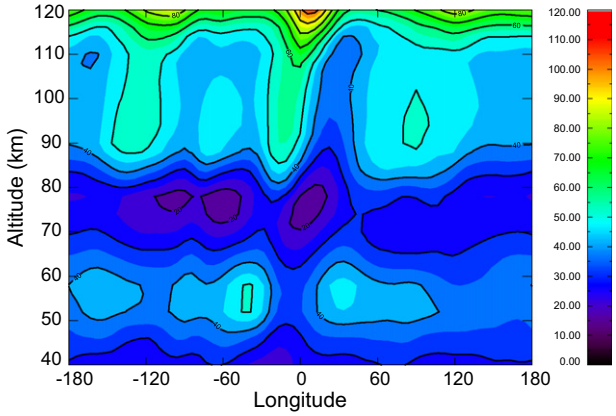

Fig. 9. Longitude–altitude variation of the difference between the predicted temperature and the CO_2 condensation temperature. Average over $L_s = 0$–$30°$, LT = 16, lat = 0°.

density in the lower thermosphere (about 120 km of altitude). A prominent longitudinal variation in the measured density was found (Keating et al., 1998). The electron density measured by MGS also shows similar longitudinal variations (Bougher et al., 2004). These variations were attributed to the effects of the propagation of non-migrating tides from the lower atmosphere (rather than to stationary waves). These non-migrating tides are created by the interaction of the solar illumination with the martian topography and to non-linear tide–tide interactions (Angelats i Coll et al., 2004).

A wave decomposition of the temperature structure predicted by the model in the equator at 78 km of altitude is shown in Fig. 10. Six non-migrating tidal components have amplitudes higher than 1.5 K at the equator, the most important components being the $(1,-2)$ (with an amplitude of 4.1 K), the $(1,-3)$ (2.3 K) and the $(1,-1)$ (1.9 K). We have used the notation (s,n), where s is the frequency (1 for diurnal tides, 2 for semidiurnal tides) and n the wavenumber, being positive for westward traveling waves. These amplitudes are sufficient to produce the longitudinal variation of temperature shown in Fig. 9. We conclude that these non-migrating waves produce the longitudinal distribution of the temperature minima predicted by the model. Through the influence of the temperature on the cloud formation, these waves are most probably also the reason behind the longitudinally confined distribution of the observed equatorial CO_2 clouds.

4.4. Mid-latitude clouds

Mid-latitude clouds have been observed mostly by THEMIS-VIS during winter in the Northern hemisphere, with some additional

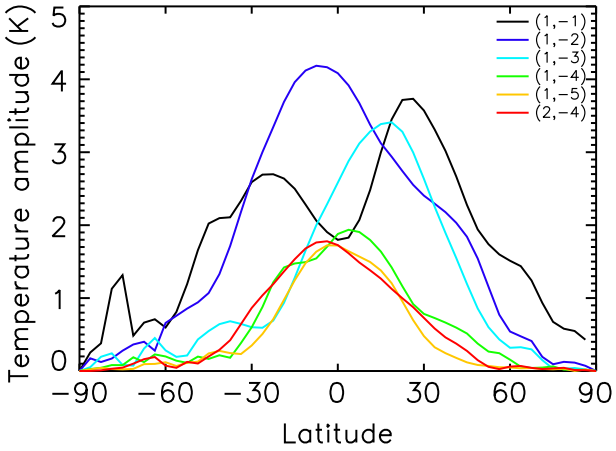

Fig. 10. Temperature amplitude (K) of the six most prominent non-migrating tidal components for $L_s = 0$–$30°$ and 78 km of altitude, as a function of latitude.

observations by OMEGA and HRSC. One mid-latitude cloud has also been observed during Southern winter by OMEGA and HRSC. As for the equatorial clouds, these mid-latitude clouds seem to be confined to restricted latitudinal and longitudinal ranges. An important difference between the observations of these mid-latitude clouds and the equatorial clouds is that THEMIS-VIS observations of the mid-latitude clouds do not allow identification of their composition: they can be water ice clouds or CO_2 ice clouds. Only the two mid-latitude clouds observed by OMEGA, one in the Northern hemisphere at $L_s = 246.3°$ and another one in the Southern hemisphere at $L_s = 54.2°$, have been spectrally identified to be CO_2 ice clouds, and the altitude of the first one is not known. We will hypothesize here that these mid-latitude clouds are CO_2 ice clouds, and we will verify if the temperature predicted by the model supports this hypothesis.

Fig. 11 shows the variation of the monthly averaged atmospheric temperatures predicted by the LMD-MGCM for the $L_s = 270$–$300°$ season with latitude (lower panel, for lon = 90°W, LT = 16) and with longitude (upper panel, for lat = 45, LT = 16). The model predicts minimum temperatures at longitudes (between 60°W and 0°) and latitudes (between 30°N and 50°N) where mesospheric clouds have been observed at this season. There are two drawbacks, though. The first one is that the altitude of the minimum temperature is of about 90 km, while the altitude of these clouds measured by THEMIS-VIS varied between 45 and 60 km. The second one is that the monthly mean average temperatures predicted by the model at this local time are, at best, more than 35 K higher than the condensation temperature of CO_2. Even

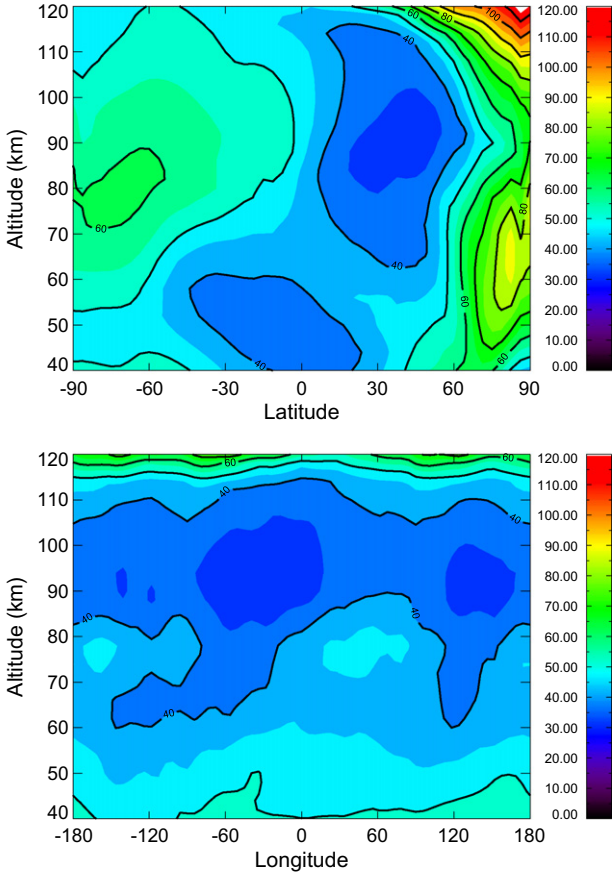

Fig. 11. Latitude–altitude (at constant lon = −60, top panel) and longitude–altitude (at constant lat = 45, lower panel) of the difference between the predicted temperature and the CO_2 condensation temperature. Average over $L_s = 270$–$300°$, LT = 16.

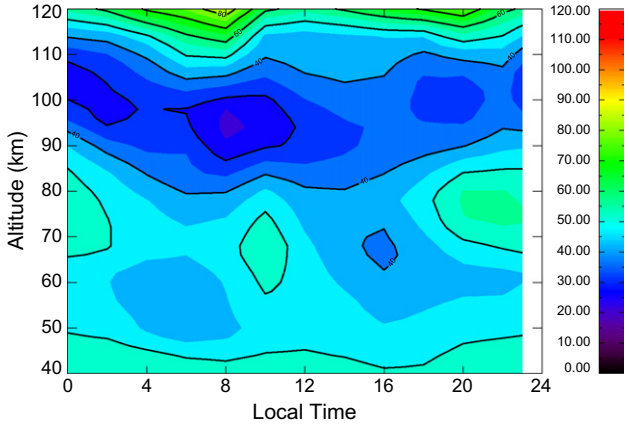

Fig. 12. Difference between the atmospheric temperature and the condensation temperature of CO_2, as a function of altitude and local time. Average over L_s = 270–300°, lon = −90°, lat = 45°.

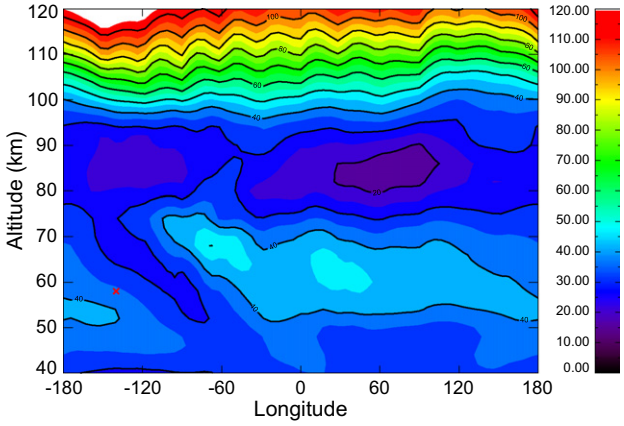

Fig. 13. Difference between the atmospheric temperature and the condensation temperature of CO_2, as a function of altitude and longitude. Average over L_s = 30–60°, lat = −48.5°, constant LT = 8.

by taking into account the day-to-day variability and the effects of gravity waves, the difference with respect to T_{cond} is too high to produce CO_2 clouds.

A look at the variability of the predicted temperature with local time and altitude (Fig. 12) shows that the minimum temperatures at the latitudes and longitudes where mesospheric clouds have been observed at this season are obtained at the beginning of the morning, around LT = 8, and at an altitude of about 95 km. At this time of the day, the temperatures are low enough to go below condensation if the day-to-day variability is taken into account (even without including the effects of gravity waves). At the local time where the clouds have been observed (around LT = 16) the model predicts a secondary minimum of temperature between 50 and 70 km, approximately, but the temperatures are too high to produce CO_2 condensation.

OMEGA observed a mid-latitude CO_2 cloud at this season, but its altitude has not been measured. At the season, latitude and longitude of this observed CO_2 cloud the model predicts temperatures close to CO_2 condensation at about 95 km, and much higher temperatures below this altitude. In the absence of a determination of the altitude of this cloud, we cannot say if the temperatures predicted by the model are in agreement or not with this observation.

We can conclude that the model predicts temperatures close to condensation at the season, latitude and longitude where THEMIS-VIS has observed mid-latitude mesospheric clouds, but the minimum temperatures are predicted to be too high in the atmosphere when compared with observations, and at a different local time.

In short, the temperatures predicted by the model do not support the hypothesis that the mid-latitude mesospheric clouds observed by THEMIS-VIS are CO_2 clouds. This opens two possibilities. The first one is that these observed clouds are water ice clouds. Further radiative transfer modeling efforts with the THEMIS-VIS observations might shed some light over the nature of these clouds. The second possibility is that the LMD-MGCM is not correctly predicting the mesospheric temperatures, and in particular the structure of the thermal tide at this particular latitude and season. Let us explore further this possibility.

A previous comparison has been made between the LMD-MGCM prediction (for MY 24) and TES MY 26 observations of temperatures at 5.28 Pa (approximately 45 km of altitude) and LT = 14 (Millour and Forget, 2008). The average difference is rather small, less than 2 K. But locally the difference between the predicted and the observed temperature can be much higher than this. In particular, at the location of the observed mid-latitude clouds (latitudes between 40–60°N and L_s = 240–300°) the model tends to overestimate the atmospheric temperature by between 10 and 20 K. This is also the case if TES MY 24 temperatures are considered. This suggests a systematic overestimation of the predicted temperatures at this particular location, altitude, and time of the year. Different factors may be producing this difference between the model and the measured temperatures. The radiative effects of water ice clouds, not included in the present version of the LMD-MGCM and abundant in the lower atmosphere at this latitude range and time of the year, are one of them (Madeleine et al., 2011). An update of the radiative properties of the dust to the latest measured values has also been shown to improve the comparison with the observations (Forget et al., 2011). Another option is the rather simple description of the altitude of the top of the dust layer included in the simulations, and that has been shown to affect the temperatures in the middle atmosphere (Forget et al., 2011). A more specific study focused specifically on this latitude and L_s range is needed.

HRSC and OMEGA also observed a mid-latitude CO_2 cloud in the Southern hemisphere during Northern spring, with an altitude between 53 and 62 km. The T_{diff} predicted by the model at lat = 48.5°S during the L_s = 30–60° period is shown in Fig. 13 as a function of longitude and temperature. Temperatures close to condensation are found at an altitude of about 90 km. The location of the observed cloud (marked with a red cross in the figure)[1] is close to a local minimum of temperature predicted by the model, but the temperatures there are not low enough to allow for CO_2 condensation, even if day-to-day variability and gravity waves perturbations are taken into account. The comparison with TES temperatures shows that again the model overestimates the temperatures between 5 and 10 K at these latitudes and times of the year at about 45 km of altitude.

5. Winds: observations and GCM results

Even more scarce than the measurements of the temperatures in the upper atmosphere of Mars are the measurements of mesospheric winds. No instrument has measured them from orbit, the only measurements being ground-based observations using the Doppler-shift technique (Lellouch et al., 1991; Sonnabend et al., 2006; Cavalié et al., 2008; Moreno et al., 2009). The models that study the dynamics of this atmospheric region remain basically unconstrained. This makes the measurements of winds obtained

[1] For interpretation of color in Figs. 1–3 and 5–14, the reader is referred to the web version of this article.

by stereo observations of mesospheric clouds by HRSC and THEMIS-VIS of high interest to validate the predictions of the models. In this section, we compare the winds measured by these two instruments with the predictions of the GCM.

We divide the wind measurements by THEMIS-VIS and HRSC in different seasonal ranges: $L_s = 0–30°$, $L_s = 30–60°$, $L_s = 90–120°$, $L_s = 210–240°$ and $L_s = 270–300°$. Most of the HRSC observations concentrate in the $L_s = 0–30°$ season, with a few measurements in the $L_s = 30–60°$ and $L_s = 90–120°$ seasons. For the $L_s = 210–240°$ and $L_s = 270–300°$ seasons we only have THEMIS-VIS measurements. All the measurements were made close to a local time of 16 h. In most of the seasons, almost all the observations concentrate in a narrow longitudinal and latitudinal corridor, which eases the comparison with the model. For more details about these measurements, we refer the reader to Määttänen et al. (2010), McConnochie et al. (2010) and Scholten et al. (2010).

Määttänen et al. (2010) already compared the winds measured by HRSC in the $L_s = 0–30°$ season with the predictions of the LMD-MGCM, finding a good agreement between the model and the observations, so we will not include that season in this study. We extend here that previous study to include all other seasons.

We plot in Fig. 14 the wind profiles predicted by the LMD-MGCM for each of the seasons under study at LT = 16 and at the latitude and longitude where most of the wind measurements have been made for that particular season. The thick black dashed line represents the seasonally averaged predicted wind, while the thin color lines are the wind profiles for the different days in that season. The symbols represent the wind measurements (crosses for HRSC and squares for THEMIS-VIS). In all seasons, the model predicts a strong day-to-day variability inside the season, which can be as strong as almost 150 m/s for the $L_s = 210–240°$ season. This variability exceeds the 1-sigma standard deviation, represented by the dashed-dotted black lines.

In general, the model predicts correctly the wind magnitude for the different seasons. This is especially true for the $L_s = 270–300°$ season, where the measured winds are always eastward, with intensity between around 0 and 130 m/s and an average value of about 60 m/s. This is almost exactly the same range and average of the winds predicted by the model. For this season, the observations suggest a decrease of the intensity of the eastward winds with increasing altitude that is also predicted by the model.

For the $L_s = 30–60°$ season the model reproduces well the observations by HRSC, which show rather weak winds with magnitudes between about −30 and 15 m/s, but not the THEMIS-VIS observations, with stronger westward winds between −50 and −70 m/s. The differences between the wind measured by HRSC and THEMIS-VIS at about the same latitude, longitude, altitude and local time cannot be explained by the model. A previous study comparing the speed of the THEMIS-VIS equatorial clouds to the zonal wind predicted by the Mars-WRF GCM (McConnochie et al., 2010) shows a similar result, with predicted winds weaker than observed. The effects of small scale processes were evoked as a possible reason of this discrepancy in McConnochie et al. (2010), together with a misrepresentation of the diurnal tide in their model.

For the $L_s = 90–120°$ season both instruments observe westward winds with magnitudes between 40 and 90 m/s at about 60 km. The predictions of the model fit well with THEMIS-VIS observations. Although a group of three THEMIS-VIS observations at about 80 km of altitude show very low wind speeds, well below the aver-

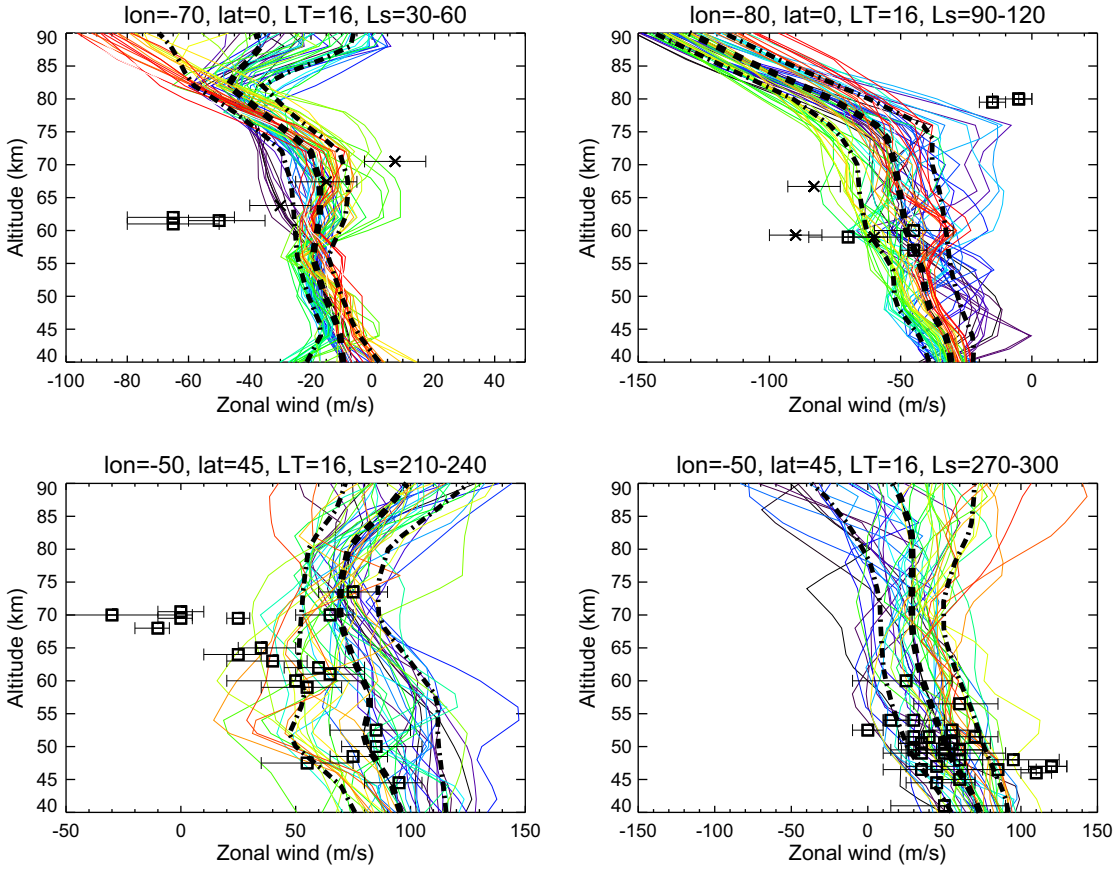

Fig. 14. Wind profiles predicted by the LMD-MGCM and winds measured by HRSC (crosses) and THEMIS-VIS (squares) for different seasons, with their error bars. Errors in the altitude determination are small (usually around ±2 km), and have not been added for the sake of clarity. For each season, the same local time, longitude and latitude are used to plot the different profiles. Thick black dashed line: seasonally averaged predicted wind. Thin color lines: daily predicted wind profiles. Black dashed-dotted lines: 1-sigma standard deviation.

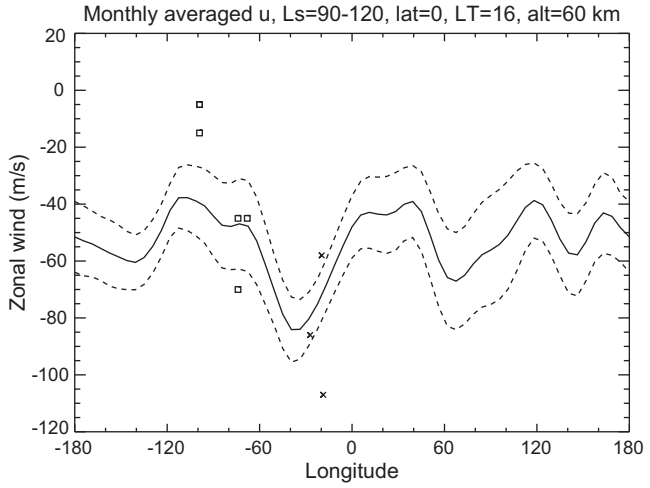

Fig. 15. Seasonally averaged wind (solid line), ±1-sigma standard deviation (dashed lines) for the L_s = 90–120 season at the equator, local time = 16 and 60 km of altitude, together with the wind measured by HRSC (crosses) and THEMIS-VIS (squares).

age wind predicted by the LMD-MGCM, some daily profiles predicted by the model show similar values at that altitude. Apparently, the winds measured by HRSC at about 60 km are more intense than predicted (and that observed by THEMIS-VIS). However, this is due to the different longitude of the THEMIS-VIS and HRSC observations. While all the THEMIS-VIS observations for this season concentrate around lon = 80°W, HRSC observations are located at longitude close to 0°. As shown in Fig. 15, the model predicts a longitudinal variation of the winds, with winds close to lon = 0° about 50 m/s stronger than those for lon = 80°W. Such a longitudinal variability is seen also in the observations.

For the period L_s = 210–240°, again the model reproduces well the winds measured by THEMIS-VIS, with most of the observations inside the range of variability predicted by the model. However, there is a group of four observations at an altitude of about 70 km which show a reduced wind intensity, or even a reversal of the predominant eastward winds to westward wind, which is not predicted by the model. This strong variability at this altitude is much stronger than that predicted by the LMD-MGCM. Again, a similar problem was found when comparing these wind measurements with the Mars-WRF GCM (McConnochie et al., 2010).

In summary, the model seems to predict well the seasonal variability of the winds observed, with westward winds in the L_s = 30–60° and L_s = 90–120° seasons and dominant eastward winds in the L_s = 210–240° and L_s = 240–270° seasons. In general, the average wind predicted by the model in each season is in agreement with the average observed winds. Given the absence of previous measurements of mesospheric winds with a good spatial coverage and vertical resolution, these are the first indications (together with the comparisons performed by Määttänen et al. (2010)) that the mesospheric dynamics predicted by the LMD-MGCM is correct, at least to a first order. However, during some seasons the measured winds show a strong variability that is not well reproduced by the model.

6. Conclusions

We have compared the mesospheric temperatures and winds predicted by the LMD-MGCM with the information obtained from the observations of mesospheric clouds. The presence of a mesospheric CO_2 cloud impose constraints on the mesospheric temperatures, given that for a CO_2 cloud to form atmospheric temperature has to be below condensation temperature of CO_2. These mesospheric clouds have only been observed at particular seasons, latitudes, longitudes, altitudes and local times. We have checked if the LMD-MGCM predicts particularly low temperatures at these locations. Some of the instruments that have observed these clouds are able to track their movement in the zonal direction, measuring their zonal speed, which can be identified to the zonal wind speed. These are the first measurements of mesospheric winds from orbit, providing a very useful dataset to validate the mesospheric dynamics predicted by the model.

While the large-scale daytime temperatures predicted by the model are usually above condensation, additional perturbations by small-scale processes, such as the propagation of gravity waves produced in the lower atmosphere up to the mesosphere, may produce local excursions of temperature below condensation in those regions where the predicted GCM temperatures are only some Kelvins above condensation. The seasonal and latitudinal location of these low temperature areas predicted by the model corresponds to a first order with the two populations of observed mesospheric clouds: equatorial clouds, observed in the first part of the martian year, and mid-latitude clouds, around the Northern winter solstice.

For the equatorial clouds, the model predicts temperatures close to condensation at the altitude, latitude, longitude and local time location of the clouds. It is shown that the different altitudes of the daytime and nighttime clouds, as well as their location close to the equator, correspond well to a similar behavior of the predicted temperatures due to the characteristics of the diurnal thermal tide. Their location at a restricted longitudinal range is also found in the temperature structure predicted by the model, due to the effects of topography interacting with the solar forcing to create non-migrating tides.

For the mid-latitude clouds, the model predicts low temperatures at their latitudinal and longitudinal location. However, the lowest temperature is predicted by the model in the early morning, and not in the afternoon, where clouds have been observed, and at a much higher altitude than the clouds have been observed. At the altitude and local time of the observed clouds the temperatures are too high to produce CO_2 condensation. Previous comparisons with temperatures measured by TES shows that the model overestimates the temperatures between 5 and 20 K at the location of the mid-latitude clouds due in part to the neglect of the radiative effects of water ice clouds in the present version of the model.

We have also compared the zonal winds predicted by the LMD-MGCM with the measurements made by stereo observations of the mesospheric clouds by THEMIS-VIS and HRSC. In general, the model predicts well the direction and the magnitude of the winds, providing a first validation of the predicted mesospheric dynamics. However, at some seasons the observations show a higher variability than predicted by the model.

Acknowledgments

The authors thank Dr. McConnochie and an anonymous referee for their comments, which contributed to significantly improve the paper. F.G.G. is partially funded by the Spanish Ministry of Science under Project AYA2008-03498/ESP and by EC FEDER funds.

References

Angelats i Coll, M., Forget, F., López-Valverde, M.A., Read, P.L., Lewis, S.R., 2004. Upper atmosphere of Mars up to 120 km: Mars Global Surveyor accelerometer data analysis with the LMD General Circulation Model. J. Geophys. Res. 109, E01011.

Angelats i Coll, M., Forget, F., López-Valverde, M.A., González-Galindo, F., 2005. The first Mars thermospheric General Circulation Model: The martian atmosphere from the ground to 240 km. Geophys. Res. Lett. 32, L04201.

Bougher, S.W., Engel, S., Hinson, D.P., Murphy, J.R., 2004. MGS Radio Science electron density profiles: Interannual variability and implications for the martian neutral atmosphere. J. Geophys. Res. 109, E03010.

Cavalié, T. et al., 2008. Vertical temperature profile and mesospheric winds retrieval on Mars from CO; Millimeter observations. Comparison with General Circulation Model predictions. Astron. Astrophys. 489, 795–809.

Clancy, R.T., Sandor, B.J., 1998. CO_2 ice clouds in the upper atmosphere of Mars. Geophys. Res. Lett. 25, 489–492.

Clancy, R.T., Wolff, M., Whitney, B., Cantor, B., 2004. The distribution of high altitude (70 km) ice clouds in the Mars atmosphere from MGS TES and MOC limb observations. Bull. Am. Astron. Soc. 36, 1128 (abstract).

Clancy, R.T., Wolff, M.J., Whitney, B.A., Cantor, B.A., Smith, M.D., 2007. Mars equatorial mesospheric clouds: Global occurrence and physical properties from Mars Global Surveyor Thermal Emission Spectrometer and Mars Orbiter Camera limb observations. J. Geophys. Res. 112, E04004.

Colaprete, A., Toon, O.B., 2002. Carbon dioxide snow storms during the polar night on Mars. J. Geophys. Res. 107, E7, CiteID 5051.

Colaprete, A., Haberle, R.M., Toon, O.B., 2003. Formation of convective carbon dioxide clouds near the south pole of Mars. J. Geophys. Res. 108, E7, CiteID 5025.

Colaprete, A., Barnes, J.R., Haberle, R.M., Montmessin, F., 2008. CO2 clouds, CAPE and convection on Mars: Observations and General Circulation Modeling. Planet. Space Sci. 56, 150–180.

Forget, F. et al., 1999. Improved General Circulation Models of the martian atmosphere from the surface to above 80 km. J. Geophys. Res. 104, 24155–24176.

Forget, F. et al., 2009. Density and temperatures of the upper martian atmosphere measured by stellar occultations with Mars Express SPICAM. J. Geophys. Res. 114, E01004.

Forget, F., Hourdin, F., Talagrand, O., 1998. CO_2 snow fall on Mars: Simulation with a General Circulation Model. Icarus 131, 302–316.

Forget, F. et al., 2011. Back to the basics: Improving the prediction of temperature, pressure and winds in the LMD General Circulation Model. Paper presented at 4th International Workshop on Mars Atmosphere: Modeling and Observations, Paris, France.

Formisano, V., Maturilli, A., Giuranna, M., D'Aversa, E., López-Valverde, M.A., 2006. Observations of non-LTE emission at 4–5 microns with the planetary Fourier spectrometer abord the Mars Express mission. Icarus 182, 51–67.

González-Galindo, F., Forget, F., López-Valverde, M.A., Angelats i Coll, M., Millour, E., 2009. A ground-to-exosphere martian General Circulation Model: 1. Seasonal, diurnal, and solar cycle variation of thermospheric temperatures. J. Geophys. Res. 114, E04001.

Inada, A., Richardson, M.I., McConnochie, T.H., Strausberg, M.J., Wang, H., Bell, J.F., 2007. High-resolution atmospheric observations by the Mars odyssey thermal emission imaging system. Icarus 192, 378–395.

Ivanov, A.B., Muhleman, D.O., 2001. Cloud reflection observations: Results from the Mars Orbiter Laser Altimeter. Icarus 154, 190–206.

James, Philip B., Kieffer, Hugh H., Paige, David A., 1992. The seasonal cycle of carbon dioxide on Mars. In: Kieffer, Hugh H., Jakosky, Bruce M., Snyder, Conway W., Matthews, Mildred S. (Eds.), Mars. University of Arizona Press, pp. 934–968, ISBN: 0-8165-1257-4.

Keating, G.M. et al., 1998. The structure of the upper atmosphere of Mars: In situ accelerometer measurements from Mars Global Surveyor. Science 279, 1672–1676.

Lee, C. et al., 2009. Thermal tides in the martian middle atmosphere as seen by the Mars Climate Sounder. J. Geophys. Res. 114, E03005.

Lellouch, E., Rosenqvist, J., Goldstein, J.J., Bougher, S.W., Paubert, G., 1991. First absolute wind measurements in the middle atmosphere of Mars. Astrophys. J. 383, 401–406.

Lewis, S.R. et al., 1999. A climate database for Mars. J. Geophys. Res. 104, 24177–24194.

López-Valverde, M.A., González-Galindo, F., López-Puertas, M., 2011. Revisiting the thermal balance of the mesosphere of Mars. Paper presented at 4th International Workshop on Mars Atmosphere: Modeling and Observations, Paris, France.

Määttänen, A., Montmessin, F., Gondet, B., Scholten, F., Hoffman, H., González-Galindo, F., Spiga, A., Forget, F., Hauber, E., Neukum, G., Bibring, J.-P., Bertaux, J.-L., 2010. Mapping the properties of the mesospheric CO_2 clouds observed by Mars Express: OMEGA and HRSC observations and a comparison to the LMD-MGCM. Icarus 209, 452–469.

Madeleine, J.-B., Forget, F., Millour, E., 2011. Modelling radiatively active water-ice clouds: Impact on the thermal structure and water cycle. Paper presented at 4th International Workshop on Mars Atmosphere: Modeling and Observations, Paris, France.

McConnochie, T.H. et al., 2005. THEMIS-VIS measurements of the altitude and velocity of clouds in the martian mesosphere. Paper presented at AGU 2005 Fall Meeting, USA, pp. P21–E03.

McConnochie, T.H., Bell III, J.F., Savransky, D., Wolff, M.J., Toigo, A.D., Wang, H., Richardson, M.I., Christensen, P.R., 2010. THEMIS-VIS observations of clouds in the martian mesosphere: Altitudes, wind speeds, and decameter-scale morphology. Icarus 210, 545–565.

Millour, E., Forget, F., 2008. Mars climate database version 4.3 validation.

Montmessin, F. et al., 2007. Hyperspectral imaging of convective CO_2 ice clouds in the equatorial mesosphere of Mars. J. Geophys. Res. 112, CiteID E11S90.

Montmessin, F., Bertaux, J.-L., Quémerais, E., Korablev, O., Rannou, P., Forget, F., Perrier, S., Fussen, D., Lebonnois, S., Rébérac, A., Dimarellis, E., 2006. Subvisible CO_2 ice clouds detected in the mesosphere of Mars. Icarus 183, 403–410.

Moreno, R., Lellouch, E., Forget, F., Encrenaz, T., Guilloteau, S., Millour, E., 2009. Wind measurements in Mars' middle atmosphere: IRAM Plateau de Bure interferometric CO observations. Icarus 201, 549–563.

Noel, V., Hertzog, A., Chepfer, H., 2009. CALIPSO observations of wave-induced PSCs with near-unity optical depth over Antarctica in 2006–2007. J. Geophys. Res. 114, D05202.

Pettengill, Gordon H., Ford, Peter G., 2000. Winter clouds over the north martian polar cap. Geophys. Res. Lett. 27, 609–612.

Pollack, James B., Haberle, Robert M., Schaeffer, J., Lee, H., 1990. Simulations of the general circulation of the martian atmosphere. 1. Polar processes. J. Geophys. Res. 95, 1447–1473.

Scholten, F., Hoffmann, H., Määttänen, A., Montmessin, F., Gondet, B., Hauber, E., 2010. Concatenation of HRSC color and OMEGA data for the determination of 3D-parameterization of high-altitude CO_2 clouds in the martian atmosphere. Planet. Space Sci. 58, 1207–1214.

Sonnabend, G., Sornig, M., Krötz, P.J., Schieder, R.T., Fast, K.E., 2006. High spatial resolution mapping of Mars mesospheric zonal winds by infrared heterodyne spectroscopy of CO_2. Geophys. Res. Lett. 33, L18201.

Spiga, A., Forget, F., 2009. A new model to simulate the martian mesoscale and microscale atmospheric circulation: Validation and first results. J. Geophys. Res. 114, E02009.

Spiga, A., González-Galindo, F., Forget, F., López-Valverde, M.A., 2011. Martian mesospheric CO_2 clouds and gravity wave activity. Paper presented at 4th International Workshop on Mars Atmosphere: Modeling and Observations, Paris, France.

Tobie, G., Forget, F., Lott, F., 2003. Numerical simulation of the winter polar wave clouds observed by Mars Global Surveyor Mars Orbiter Laser Altimeter. Icarus 164, 33–49.

Washburn, E.W., 1948. International Critical Tables of Numerical Data, Physics, Chemistry, and Technology, vol. 3. McGraw Hill, New York.